

SOLITONS

PACS numbers: 42.65.Tg; 42.65.Sf; 42.60.Da
DOI: 10.1070/QE2005v035n03ABEH002786

Dynamics of strong coupling formation between laser solitons

N.N. Rosanov, S.V. Fedorov, A.N. Shatsev

***Abstract*. The dynamics of the strong coupling formation between two solitons with the unit topological charge is studied in detail for a wide-aperture class A laser. The sequence of bifurcations of the vector field of energy fluxes in the transverse plane was demonstrated during the formation of a soliton complex.**

Keywords: *solitons, nonlinear dynamics, bifurcation.*

Solitons in a wide-aperture laser with a saturable absorber predicted in [1] and theoretically and numerically studied in detail in [2 – 4] (see also important experimental and calculated results presented in [5]) belong to dissipative (not conservative) optical solitons. The properties of solitons of these two types, conservative and dissipative, are fundamentally different, a strong suppression of the noise and drift of parameters of dissipative solitons making them promising for optical data processing.

The study of the interaction between solitons is important for the development of their theory and potential applications. The case of a weak coupling between solitons with a weak overlap of the fields from individual solitons can be analysed more simply [6]. However, as shown in [7] (see also [2 – 4]), laser solitons can also form more complicated, strongly coupled structures, which cannot be decomposed into individual solitons. Even more unusual is the localised structure of laser radiation obtained in calculations [8], in which different parts can be coupled weakly or strongly, their rotating being with different angular velocities. According to [9], the quantitative criterion for strong or weak coupling is related to the bifurcations of the topological structure of transverse energy fluxes. Some examples of such bifurcations are presented in [9]. The aim of our paper is to analyse in more detail the bifurcations of the topological structure of the Poynting vector during the formation of a strongly coupled pair of vortex laser solitons with coinciding (unit) topological charges.

As in [2 – 4, 9], we will consider a wide-aperture (with a rather large Fresnel number) class A laser (relaxation times in the medium are much shorter than the time of field establishment in the resonator) with plane – parallel mirrors and an intracavity saturable absorber. In the average-field approximation, the equation for the envelope of the electric field strength E has the form

$$\frac{\partial E}{\partial t} = (\mathrm{i} + d)\Delta_\perp E + Ef\left(|E|^2\right). \tag{1}$$

Here, $\Delta_\perp = \nabla_\perp^2 = \partial^2/\partial x^2 + \partial^2/\partial y^2$ is the transverse Laplace operator; d is the effective diffusion coefficient characterising a weak spatial dispersion of the medium ($0 < d \ll 1$); and the time is normalised to the photon lifetime in an empty resonator. The function $f(I)$ of the radiation intensity $I = |E|^2$ describes the intertialess saturation of the gain and absorption. By neglecting frequency detunings, this function is real and has the form

$$f\left(|E|^2\right) = -1 + \frac{g_0}{1 + |E|^2} - \frac{a_0}{1 + b|E|^2}. \tag{2}$$

We used in calculations the following values of the parameters: the small-signal gain $g_0 = 2.11$, the small-signal absorption coefficient $a_0 = 2$, the ratio of saturation gain and absorption intensities $b = 10$, and the diffusion coefficient $d = 0.06$. For the localised structures under study, the field at infinity should vanish.

The simplest two-dimensional laser solitons have the axially symmetric intensity distribution. In the polar coordinates r and φ, we have

$$E = A(r)\exp(\mathrm{i}m\varphi)\exp(-\mathrm{i}\nu t). \tag{3}$$

The integer $m = 0, \pm 1, \pm 2, \ldots$ is called the topological index. The radiation wave front for $m = 0$ is regular and has screw dislocations (optical vortices) when $m \neq 0$. The frequency shift ν and the complex radial function $A(r)$, which play the roles of the eigenvalue and the eigenfunction, respectively, are determined by the numerical solution of the radial equation following from (1) [2, 3]. The stability of axially symmetric localised structures with respect to small perturbations is analysed in a standard way [2]. The parameters used in calculations correspond to the stability region of the axially symmetric solitons. The total instant phase $\Psi = \arg E$ consists of the radial phase $\Psi_0(r) = \arg A$ and the angular component

$$\Psi(r, \varphi) = \Psi_0(r) + m\varphi. \tag{4}$$

N.N. Rosanov, S.V. Fedorov, A.N. Shatsev Research Institute for Laser Physics, Birzhevaya lin. 12, 199034 St. Petersburg, Russia;
e-mail: rosanov@ilph.spb.su

Received 12 July 2004; revision received 16 December 2004
Kvantovaya Elektronika **35** (3) 268 – 272 (2005)
Translated by M.N. Sapozhnikov

Because the constant component of the phase is insignificant, we can assume that $\Psi_0(0) = 0$.

The initial (at the instant $t = 0$) field distribution was represented as a superposition of the fields of two axially symmetric solitons with the topological indices $m_1 = m_2 = 1$:

$$E = A(r_1)\exp[\mathrm{i}\Psi_0(r_1) + \mathrm{i}\varphi_1] + A(r_2)\exp[\mathrm{i}\Psi_0(r_2) + \mathrm{i}\varphi_2 + \mathrm{i}\vartheta]. \quad (5)$$

Here, ϑ is the constant phase difference; r_n and φ_n ($n = 1, 2$) are the two sets of polar coordinates whose centres coincide with the centres of the nth soliton, and the distance between the coordinate centres is L:

$$r_n^2 = \left(x \pm \frac{L}{2}\right)^2 + y^2,\ \cos\varphi_n = \left(x \pm \frac{L}{2}\right)\frac{1}{r_n},\ \sin\varphi_n = \frac{y}{r_n}. \quad (6)$$

The numerical solution of Eqn (11) with the initial condition (5) by the splitting method using the fast Fourier transform algorithm gives the evolution of the field structure.

Within the framework of the adopted quasi-optical approach for the fixed (linear) polarisation of radiation, the transverse components $\boldsymbol{S}_\perp = \{S_x, S_y\}$ of the Poynting vector averaged over the optical cycle are determined at each instant t by the slowly varying complex amplitude (envelope) E or by the real amplitude $A = |E|$ and the phase $\Psi = \arg E$:

$$\boldsymbol{S}_\perp = A^2\nabla_\perp\Psi = \mathrm{Im}(E^*\nabla_\perp E). \quad (7)$$

The streamlines for these components – the curves with the tangents to them at each x, y point coinciding in direction with the vector $S_\perp$, are determined by the equations

$$\frac{\mathrm{d}x}{S_x(x,y)} = \frac{\mathrm{d}y}{S_y(x,y)}. \quad (8)$$

By introducing the parameter τ changing along the curve length, these equations can be represented in a more convenient form

$$\frac{\mathrm{d}x}{\mathrm{d}\tau} = S_x(x,y),\ \frac{\mathrm{d}y}{\mathrm{d}\tau} = S_y(x,y). \quad (9)$$

The transverse distributions of the Poynting vector and intensity uniquely describe the field (accurate to an insignificant constant phase).

Equations of type (9) have been studied in detail in the theory on nonlinear oscillations [10]. To find the structure of their phase-plane partition into cells with trajectories $x(\tau)$, $y(\tau)$ of the same type, first the singular (stationary) points (x_0, y_0) should be found at which $S_x(x_0, y_0) = 0$ and $S_y(x_0, y_0) = 0$ simultaneously. Then, the type of 'stability' of the points was determined by the linearization of expressions (9) near these points. The quotation marks indicate that we are dealing not with the temporal stability (the instant of time t is fixed) but with the type of solutions for $\tau \to \infty$. In the general case, to divide the phase plane into cells, it is also necessary to know nonlocal elements, namely, the limit cycles (closed trajectories with x and y periodically varying upon variation of τ) and the location of the separatrices of saddles [10]. They are determined by solving (9) numerically. In this case, the topological structure of energy fluxes at the instant of time t is determined uniquely. However, this structure can change qualitatively with time, which corresponds to its bifurcations. For equations of type (9) in nondegenerate cases, the bifurcations correspond to the following four types of nonrough elements [10]: (1) the complex equilibrium state appearing after the merging of two simple singularities; (2) the degenerate focus or centre; (3) the double limit cycle (appearing, for example, after the merging of the 'stable' and 'unstable' limit cycles; and (4) the separatrix going from one saddle to another or returning back. We will follow below the bifurcations of the structure of energy fluxes, by pointing out the corresponding numbers of these types. The temporal reconstruction of the topological structure of energy fluxes is shown in Fig. 1.

The initial (at $t = 0$) field structure is described by a linear superposition of fields of two solitons (5) with $L = 26$ and $\vartheta = \pi$. The phase plane of energy fluxes corresponding to Eqn (5) (Fig. 1) has three singularities: two foci (centres of solitons corresponding to the wave-front dislocations) and the saddle S_0 between these foci. The foci are 'stable' (as τ increases, the trajectories wind on them). Each of the foci is surrounded by three limit cycles: the 'unstable' (nearest to the corresponding focus), 'stable' (intermediate), and 'unstable' (external) cycles. The 'stable' and 'unstable' limit cycles are shown in Fig. 1 by solid and dashed curves, respectively. At the initial instant of time, the limit cycles are close to concentric circles. The separatrices emerging from the saddle tend to infinity (they are shown by dotted curves with arrows in Fig. 1), while those entering into the saddle uncoil from the external limit cycles.

For $t = 0$, the saddle separatrices and limit cycles divide the phase plane into eight cells ($N_c = 8$) with the topologically equivalent streamlines. The six of these cells have a finite area (by three at the left and right) and the two – an infinite area (the latter are separated by the separatrices emerging from the saddle). In the vicinity of the saddle S_0 of the energy streamlines, the intensity distribution is also saddle-like. Note also that the trajectories are merged in all the figures only at the stationary points or asymptotically (for $\tau \to \pm\infty$). In other cases, the apparent merging is observed due to the limited accuracy of graphic representation.

A comparison between Figs 1.1 ($t = 0$) and 1.2 ($t = 5.6$) shows that the first in time ($t < 5.6$) is the bifurcation of the third type with merging and subsequent annihilation of an external 'unstable' and intermediate 'stable' limit cycles of the left soliton ($N_c = 6$).

The type of the next bifurcation ($5.6 < t < 6$) can be determined by comparing Figs 1.2 and 1.3. The type of singularities in this time interval does not change. Only one external 'unstable' limit cycle corresponding to the right soliton disappears from limit cycles during bifurcation. The separatrix loop simultaneously emerging from the saddle, which went downwards earlier (see Fig. 1.2), covers the limit cycles of the left soliton and returns back to the saddle. After the bifurcation, this separatrix winds on a 'stable' limit cycle of the right soliton. This is a bifurcation of the fourth type. Here, $N_c = 5$, and one of the cells has an infinite area.

In passing to Fig. 1.9 ($t = 20$), the bifurcation is observed with the formation of two limit cycles: the 'stable' left cycle and the 'unstable' one, covering the 'stable' left

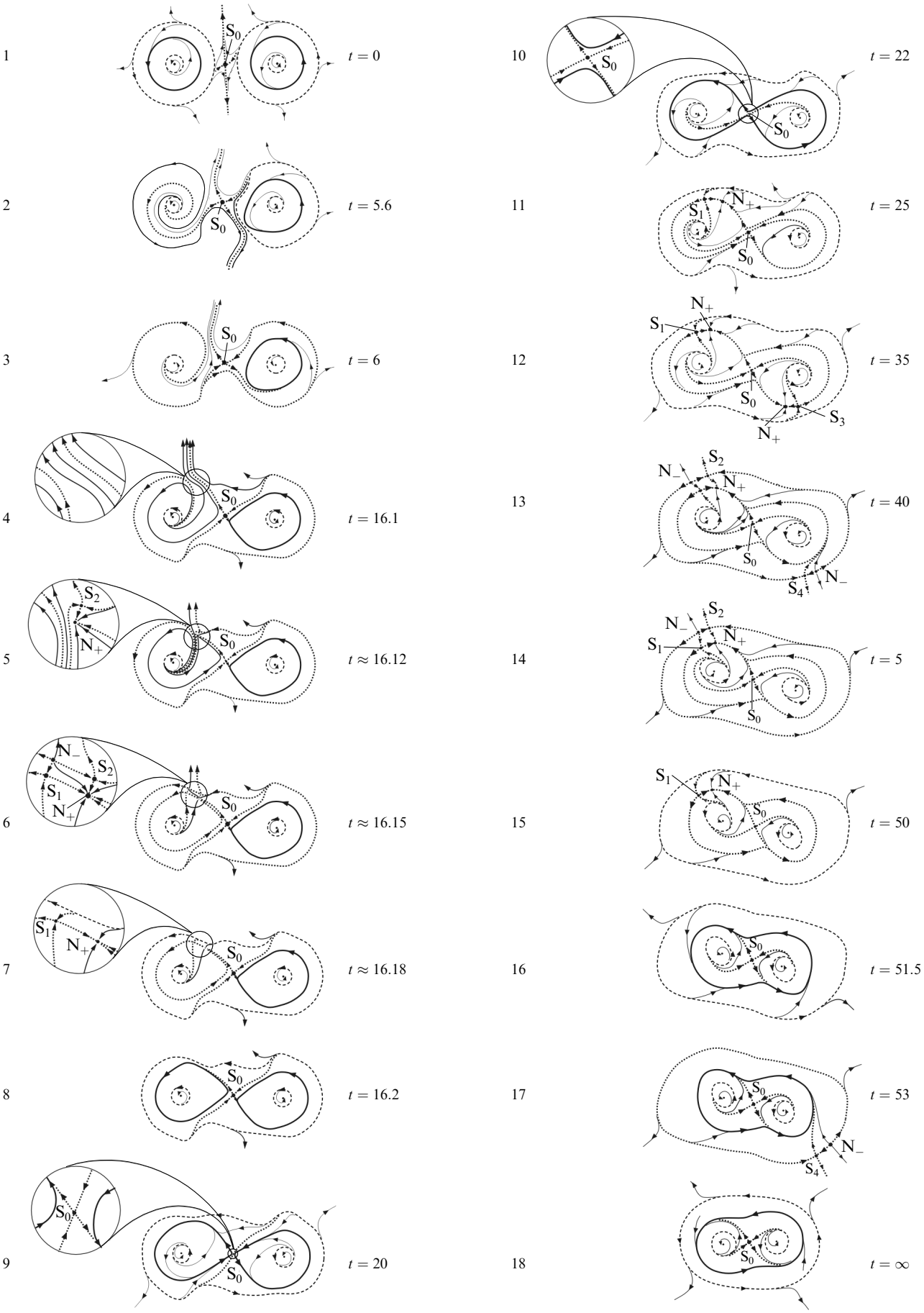

Figure 1. Series of phase portraits of energy fluxes (see the text).

and right cycles. In fact this transition occurs within a narrow time interval $16.1 < t < 16.2$. Unlike other variants, in this case it is impossible to classify this bifurcation as one of the elementary bifurcations. However, it can be represented as a sequence of several elementary bifurcations of the first type, direct and reverse, proceeding at small temporal and spatial scales, which allows their separation. Figures 1.4–1.8 show this assumed sequence with some distortions of spatial scales and insets for clearness.

Figure 1.4, which is topologically equivalent to Fig. 1.3, shows the schematic diagram of the Poynting vector for $t = 16.1$ and $N_c = 5$. In passing to Fig. 1.5, the reverse bifurcation of the first type is realised: the saddle S_2 and the 'stable' knot N_+ ($N_c = 7$) appear. Then, in passing to Fig. 1.6, the saddle S_1 and the 'unstable' knot N_- ($N_c = 9$) appear due to the reverse bifurcation. During the next bifurcation of the first type, the saddle S_2 merges with the knot N_- ($N_c = 8$) (Fig. 1.7). In this case, the limit cycle appears from the saddle–knot separatrix loop, similarly to situations depicted in Figs 1.8, 1.15, 1.16, and 1.18. Finally, by the instant of time $t = 16.2$ (Fig. 1.8), the saddle S_1 and the knot N_+ merge due to bifurcation of the first type (Fig. 1.8) and we obtain the configuration that is topologically equivalent to that presented in Fig. 1.9 ($N_c = 7$).

Note that after the appearance of two saddles and two knots, a characteristic 'tetragon of separatrices' is formed due to two reverse bifurcations of the first type (inset in Fig. 1.6). In this case, the tetragon is very small, its size being smaller than a step of the calculation network. A similar characteristic tetragon appears then for $t = 40$ and 45 as a fluctuation (see Figs 1.13 and 1.14, where it is well resolved both spatially and in time). However, for $t = 16.2$ (Figs. 1.7 and 1.8), unlike $t = 50$ (passage from Fig. 1.15 to Fig. 1.16), each of the two saddles merges again, however, not with its 'own' knot (which appeared earlier simultaneously with this saddle during the bifurcation of the first type) but with a 'foreign' knot, which drastically changes the situation. Such a 'relocking' of separatrices provides a qualitative change in the topological structure of Poynting-vector fluxes.

In passing to Fig. 1.10 ($t = 22$), two reverse bifurcations of the fourth order are simultaneously observed at the right and left (cf. the passage from Fig. 3.5c to 3.5a in [10]). During the bifurcation, the two loops of the saddle separatrices exist with one common point, as in Fig. 132 in [11] (section 29). The number of cells is $N_c = 6$ (hereafter, one of the cells has an infinite area). This configuration is already topologically equivalent to the final configuration, but the soliton complex has not formed yet.

Figure 1.11 ($t = 25$) exhibits a reverse bifurcation of the fist type – the appearance of the 'stable' knot N_+ and saddle S_1 in the inner 'stable' cycle at the top left. Here, the limit cycle is destroyed, transforming during bifurcation to the saddle–knot separatrix loop. Similar situations are depicted in Figs 1.12, 1.13, and 1.17 ($N_c = 7$).

A comparison of Figs 1.12 ($t = 35$) and 1.11 ($t = 25$) shows the presence of a reverse bifurcation of the first type – the appearance of the 'stable' knot N_+ and saddle S_3 in the external 'unstable' cycle at the bottom right ($N_c = 9$).

Figure 1.13 ($t = 40$) demonstrates three bifurcations close in time: the reverse bifurcation of the first type – the appearance of the 'unstable' knot N_- and saddle S_2 in the external 'unstable' cycle at the top left, the same bifurcation at the bottom right, and bifurcation of the first type – the merging of the 'stable' knot N_+ and saddle S_3 in the inner 'stable' cycle at the bottom right. The total number of cells is maximum and is $N_c = 10$. In passing to Fig. 1.14 ($t = 45$), a bifurcation of the first type is observed – the merging of the 'unstable' knot N_- and saddle S_4 at the point of the external unstable cycle ($N_c = 8$). Figure 1.15 ($t = 50$) shows a bifurcation of the first type – the merging of the 'unstable' knot and saddle S_2 in the external 'unstable' cycle at the top left ($N_c = 7$). In passing to Fig. 1.16 ($t = 51.5$), a bifurcation of the first type is observed – the merging of the 'stable' knot and saddle S_1 at the point of the inner 'stable' cycle ($N_c = 6$). This configuration is topologically equivalent to the final configuration. Figure 1.17 ($t = 53$) shows reverse bifurcation of the first type – the appearance of 'unstable' knot and saddle at the point of the external 'unstable' cycle at the bottom right ($N_c = 6$). The final ($t = \infty$) established configuration is shown in Fig. 1.18. The topological structure is established already at $t \approx 65$, and its shape is established after a few hundred time units. The total number of cells is $N_c = 6$.

Thus, we have studied the bifurcations of the structure of energy fluxes (the Poynting vector averaged over the optical cycle) during the formation of a strongly coupled pair of two laser vortices with identical topological charges. It should be emphasised that the control parameter in this case is time t, the trajectories of the phase plane at each instant of time corresponding to the energy streamlines, which are parametrised by the quantity τ proportional to the streamline length.

The cascade of bifurcations obtained in the paper is nontrivial. However, each unit bifurcation is among the four known bifurcations (in the case studied, only nonrough elements of the first, third, and fourth types were observed). We believe that analysis of bifurcations is useful not only for interpretation of the results obtained but also for finding new types of strongly coupled soliton complexes. Note that it is the analysis of the topological structure of the Poynting vector, in addition to a more standard description of the spatiotemporal dynamics of the electromagnetic-field envelope, that allowed us to separate the individual and collective elements of solitons (limit cycles) and to observe bifurcations consisting in the transformation of some individual limit cycles to the collective cycles during the formation of this soliton complex.

The experimental conditions for the appearance of such structures can be realised in semiconductor amplifiers and lasers [12], for example, in vertical-cavity surface-emitting lasers. For a cavity with a typical transverse size of 100 μm, a longitudinal size of 10 μm, and the effective reflectivity of mirrors $R \sim 0.1 - 0.001$, the characteristic time scale [the dimensionless time unit in (1)] will be $\sim 10^{-12} - 10^{-14}$ s. Note also that similar effects can be also observed for discrete dissipative solitons in two-dimensional networks of coupled fibres with nonlinear gain and absorption, which are promising for optical data processing [13].

Acknowledgements. This work was supported by the Russian Foundation for Basic Research (Grant Nos 04-02-16605a and 04-02-81014 Bel.)

References

1. Rosanov N.N., Fedorov S.V. *Opt. Spektrosk.*, **72**, 1394 (1992).

2. Rosanov N.N. *Spatial Hysteresis and Optical Patterns* (Berlin: Springer, 2002).
3. Fedorov S.V., Rosanov N.N., Shatsev A.N., Veretenov N.A., Vladimirov A.G. *Trans. IEEE J. Quantum Electron.*, **39** (2), 1979 (2003).
4. Rosanov N.N., Fedorov S.V., Shatsev A.N. *Opt. Spektrosk.*, **95**, 902 (2003).
5. Slekys G., Staliunas K., Weiss C.O. *Opt. Commun.*, **149**, 113 (1998).
6. Gorshkov K.A., Ostrovsky L.A. *Physica D*, **3**, 428 (1981).
7. Rosanov N.N., Fedorov S.V., Fedorov A.V., Khodova G.V. *Opt. Spektrosk.*, **79**, 868 (1995).
8. Rosanov N.N., Fedorov S.V., Shatsev A.N., Loiko N.A. *Opt. Spektrosk.*, **97**, 96 (2004).
9. Rosanov N.N., Fedorov S.V., Shatsev A.N. *Zh. Eksp. Teor. Fiz.*, **125**, 486 (2004).
10. Butenin N.V., Neimark Yu.I., Fufaev N.A. *Vvedenie v teoriyu nelineinykh kolebanii* (Introduction to the Theory of Nonlinear Oscillations) (Moscow: Nauka, 1976).
11. Andronov A.A., Leontovich E.A., Gordon I.I., Maier A.G. *Teoriya bifurkatsii dinamicheskikh system na ploskosti* (Theory of Bifurcations of Dynamic Systems on a Plane) (Moscow: Nauka, 1967).
12. Ultanir E.A., Stegeman G.I., Michaelis D., Lange C.H., Lederer F. *Phys. Rev. Lett.*, **90** (25), 253903 (2003).
13. Ultanir E.A., Stegeman G.I., Christodoulides D.N. *Opt. Lett.*, **29** (8), 845 (2004).